VOL. 18, NO. 4, FEBRUARY 2023 ISSN 1819-6608
ARPN Journal of Engineering and Applied Sciences

www.arpnjournals.com

MAGNETIC AND OPTICAL PROPERTIES OF COBALT-DOPED HEMATITE NANOPARTICLES OF LOGAS NATURAL SAND FOR ENVIRONMENTAL APPLICATION

Erwin Amiruddin[1], Salomo Sinuraya[1], Amir Awaluddin[2], Rahmondia Nanda Setiadi[1], Muhammad Rizki[3], Novalia Magdalena Purba[3] and Indah Tamara Sitorus[3]
[1]Department of Physics, Faculty of Mathematics and Natural Sciences, Riau University, Indonesia
[2]Department of Chemistry, Faculty of Mathematics and Natural Sciences, Riau University, Indonesia
[3]Magnetic Laboratory, Faculty of Mathematics and Natural Sciences, Riau University, Indonesia
E-Mail: erwin_amiruddin@yahoo.com

ABSTRACT

The cobalt doped hematite (α-Fe_2O_3) nanoparticles have been prepared by ball milling method using Logas natural sand as a raw material. The milled hematite nanoparticles were doped using cobalt with concentration of 0, 5, 10, 15 and 20 wt. %. The optical, structural and magnetic properties were studied using Uv-Vis spectroscopy, X-ray diffractometer (XRD), and vibration sample magnetometer (VSM), respectively. The optical properties strongly depend on cobalt content and showed that the band gaps of cobalt doped hematite decrease with increasing cobalt content. The samples exhibited weak ferromagnetic behaviour with the coercivity ranged from 124 Oe to 299 Oe. The XRD measurements confirmed the formation of crystalline, rhombohedral crystal structure and hematite nanoparticles. The samples show cobalt-hematite nanoparticles as indicated through XRD measurement. The average crystallite size calculated using Scherrer formula found to be 38.51, 35.67, 33.75, 32.73 and 31.53 nm after being doped with cobalt 0, 5 and 10, 15 and 20 wt. %, respectively. Some other elements such as silicon and titanium and others elements were detected, which demonstrates that these milled samples are not purely hematite as confirmed by X-Ray Fluorescence Spectroscopy (XRF) results.

Keywords: Logas natural sand, ball milling, cobalt, optical, magnetic and structural properties.

INTRODUCTION

Magnetic iron oxides have been the subject of current research since they can be obtained from natural sand [1]. These oxides exist in nature in many forms; however, the most common forms are magnetite (Fe_3O_4), hematite (α-Fe_2O_3) and maghemite (γ-Fe_2O_3) [2]. In a nanometer size, magnetic iron oxide particle has a super paramagnetic property [3] which makes them to be uses in broader application started from catalysts [4] to biomedical applications [5, 6] and environmental remediation [7]. Many different methods preparing of hematite nanoparticles such as hydrothermal [8], chemical precipitation [9], microwave, [10] and ball milling [11-13] has been currently presented. The most common method for the preparation is ball milling [14]. in this method initially larger grain sizes of the sample are reduced to nanometer scale particles by mechanical means. The advantage of using this method is simple, efficient, high yield and low cost compared to other methods. Previous researchers [14, 15] have used ball milling method to produce magnetic iron oxide nanoparticles. For example, [15] used ball milling method to prepare 39.2 nm α- Fe_2O_3 nanoparticles directly from Logas natural sand and found that the α-Fe_2O_3 nanoparticles has a hexagonal structure.

Magnetic properties, phase and morphology of the obtained particles are depended on time, speed and types of milled balls [14]. One of the most important parameters for controlling the magnetic properties of magnetic iron oxide nanoparticles is the size of the particles. However, development of a simple, reliable, and low cost methodology to prepare magnetic iron oxide nanoparticles with controllable size and size distribution remains a challenging task for researchers. According to previous researchers [16], when transition metal elements doped into nanoparticles, they alter the optical, magnetic and structural properties of the nanoparticles. Moreover, doping methodology and selection of doped element influence the optical, magnetic and structural properties of magnetic iron oxide nanoparticles. In this paper, we have investigated the optical, magnetic and structural properties of undoped and cobalt doped magnetic iron oxide particles of natural sand from Logas, Kuansing District, Riau Province using ball-milling method for environmental application.

EXPERIMENTAL PROCEDURE

Natural sand samples were collected from Logas-Kuansing Regency-Riau Province. The amount of non iron oxide particles of the samples were reduced using iron sand separator (ISS). The obtained iron oxide particles were milled using 2-stage ball milling method. The first stage of milling was last for 50 hours and followed by separation between iron oxide and non-iron oxide using strong NdFeB magnet. The second stage was last for another 50 hours and followed by separation between iron oxide and non-iron oxide using strong NdFeB magnet. The product of the 2nd ball milling process was divided into 4 parts with the same amount of weight. Each of these products was milled together with cobalt as a dopant composition of 0, 5, 10, 15 and 20 wt. % for 20 hours. Optical, magnetic and structural properties of the iron oxide nanoparticles before and after doping were studied

using Uv-Vis spectroscopy, X-ray diffractometer (XRD), and vibration sample magnetometer (VSM), respectively. The composition of the samples before and after being cobalt doped was obtained using X- Ray Fluorescence Spectrometer (XRF).

RESULTS AND DISCUSSIONS

Figure-1 shows the X-Ray diffraction (XRD) patterns of undoped and cobalt doped iron oxide (α-Fe_2O_3) nanoparticles. The Structural properties of the samples were analyzed using X-Ray Diffractometer Phillips producing CuKα radiation with wavelength (λ) of 0.15406 nm. In this measurement, the diffraction angle was selected in interval of 10^o to 70^o with the step of 0.01^o. The XRD pattern of the undoped α-Fe_2O_3 nanoparticles exhibits diffraction angles of 23.92^o, 32.74^o, 35.37^o, 40.47^o, 48.95^o, 53.38^o, 56.70^o 61.84^o and $63.50^o$and completely matched the reflections of (102), (104), (110), (113), (024), (116), (122), (214) and (300), respectively. This is agreement with literature JCPDS file number: 89-8103 with rhombohedral phase of α-Fe_2O_3 [17]. All the observed diffraction peaks have been indexed to α-Fe_2O_3. In the case of 5, 10, 15 and 20 wt. % cobalt doped α-Fe_2O_3 nanoparticles, the diffraction patterns of α-Fe_2O_3 nanoparticles show that their structure is not changed with cobalt doping. However, the XRD patterns show an additional peak at diffraction angle of 44.38^o with correspond to reflection plane of (400) cobalt [18].

In the case of 5, 10, 15 and 20 wt. % cobalt doped hematite nanoparticles, the diffraction patterns of α-Fe_2O_3 nanoparticles show that their structure is not changed with cobalt doping. The XRD patterns show additional peaks at diffraction angle of 44.38^o with correspond to reflection plane of (400) which is characteristic of cobalt (JCPDS15-0806) [19]. The intensity of the reflection of cobalt phase increases as its content increases which reveals the dominant presence of cobalt phase in the samples. Therefore, the existence of diffraction peak related to the cobalt and α-Fe_2O_3 nanoparticles showed successful formation of α-Fe_2O_3-cobalt nanoparticles using ball milling method. The average crystallite size hematite nanoparticles was calculated using Scherrer's formula [20]

$$D \frac{K\lambda}{\beta Cos\theta} \quad \text{..... (1)}$$

where D is the crystallite size (nm), λ is the X-ray wavelength (λ= 1.5406 Å), k is the Scherrer constant, which equals 0.9, β is the full width at half maximum (FWHM) of peaks and θ is the corresponding diffraction angle (degree). The estimated crystallite size of pure α-Fe_2O_3 is 38.52 nm and that of 5 wt.%, 10 wt.%, 15 wt.% and 20 wt% cobalt nanoparticles is 35.67, 33.75, 35.73 and 31.53 nm (Table-1). It can be found that the crystallite size of cobalt doped hematite nanoparticles decreases with increasing cobalt content, indicating that the addition of cobalt can effectively decrease the hematite crystalline grain growth. Therefore, the average crystallite size of cobalt doped hematite nanoparticles become smaller compared to that of the undoped hematite nanoparticles. In order to compare our results with the literature, we used all the planes in the diffraction pattern to calculate the size of the α-Fe_2O_3 crystallite. The results obtained agree with the data in the literature in which the crystallite sizes between 21 and 82 nm [21].

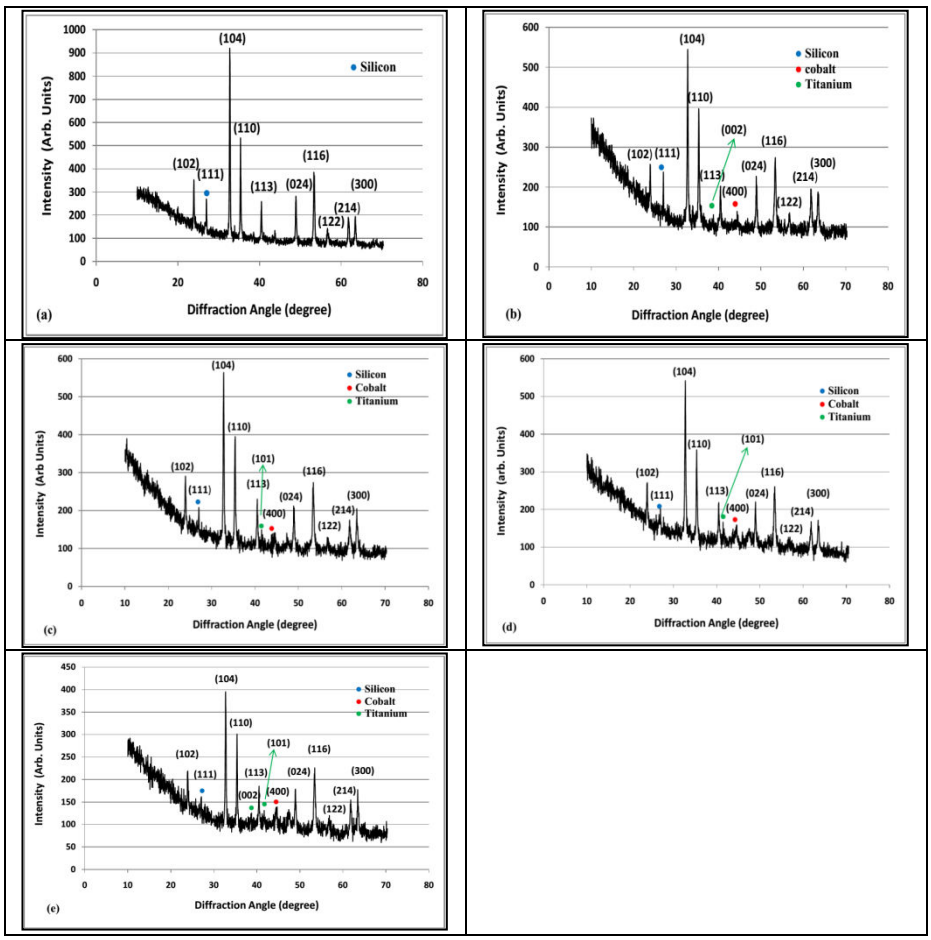

Figure-1. XRD patterns of (a) undoped and (b) 5 wt.% and (c) 10 wt.% (d) 15 wt.% and (e) 20 wt.% cobalt doped hematite nanoparticles.

Table-1. The average crystallite size of undoped and cobalt doped hematite nanoparticles.

Co Content (wt.%)	Average Crystallite size (nm)
0 (undoped)	38.51
5	35.67
10	33.75
15	32.73
20	31.53

Elemental chemical composition of Logas natural sand before and after milling process as well as after being 5 wt.% doped nickel, chromium and cobalt determined using X-Ray Fluorescence Spectroscopy (XRF) is presented in Figure-2. It can be seen that the XRF data clearly evidence the occurrence of the doping elements. The figure also indicates that the α-Fe_2O_3 nanoparticles are not free from impurity elements. The Fe contents were increased very significantly after milling (100 hours). Some other elements for examples Al, Si, and other elements were decreased, however, the other elements such as Ti increases. This indicates that natural sand grains break into smaller parts so that the non-magnetic and magnetic grains were separated during milling process. Moreover, Fe and Ti elements cannot be separated until 120 hours milling process suggesting that Fe and Ti exist in the form of compound.

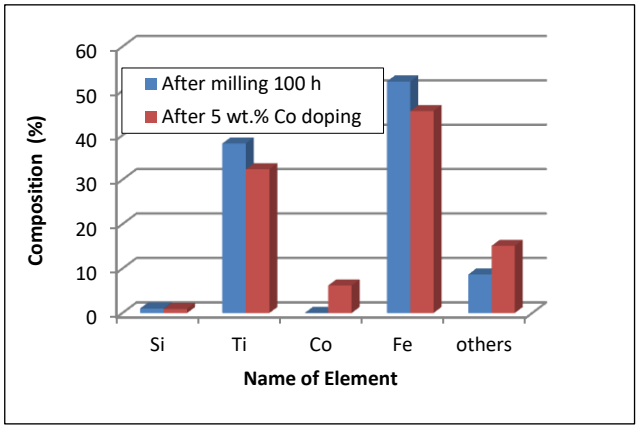

Figure-2. Elemental chemical composition of sample before and after being milled for 100 hours and fter being 5 wt.% doped cobalt observed by XRF.

The plots of applied magnetic field (Oe) vs magnetization (emu/g) of the undoped and chromium doped hematite nanoparticles are given in Figure-3. These loops were measured using vibration sample

magnetometer (VSM) in which the applied magnetic field used was ranging from +20.000 Oe to -20.000 Oe. The saturation magnetization value of the samples increases as the cobalt content increase which might be because of the presence of more cobalt atoms at the grain boundaries as revealed in the X-Ray Diffraction results as indicates in Figure-1. The measured magnetic parameters such as saturation magnetization (Ms), remanence magnetization (Mr), coercivity (Hc) and loop squareness are given in Table-2. It is found that saturation magnetization of undoped hematite nanoparticles is 0.65 emu/g. This value is lower than that reported by previous researcher [22]. The increase in saturation magnetization values compared to undoped hematite nanoparticles is associated with an increase in cobalt content of the sample which is clearly as magnetic element.

The hysteresis loops of all samples show weak ferromagnetic behavior characterized by their low coercivity value as shown in Figure-3. The coercivity of the undoped hematite nanoparticles is about 124 Oe and increases to 221, 255 and 299 Oe for cobalt doped hematite with cobalt content of 5, 10 and 15 wt.5, respectively. Thus the increase of coercivity in this range of cobalt content can be qualitatively understood in terms of the effect of relatively tightly coupled iron oxide nanoparticles followed by the increase in iron oxide nanoparticles separation, which ultimately reduces exchange coupling between weakly coupled iron oxide nanoparticles or clusters [23]. The corcivity value of the sample reduces to 269 Oe for cobalt content 20 wt. %. The reduction of the coercivity value is due to more interaction between magnetic (cobalt) nanoparticles in the sample. This effect could certainly lead to the decrease in the coercivity for the samples with cobalt content of 20 wt. % as indicated in Table-2. The remanent magnetization (M_r) value of the undoped hematite nanoparticles is about 0.095 emu/g and it increases to 1.71 emu/g for 15 wt.% cobalt content and decreases to 0.145 emu/g for cobalt content of 20 wt.% as shown in Table-2.

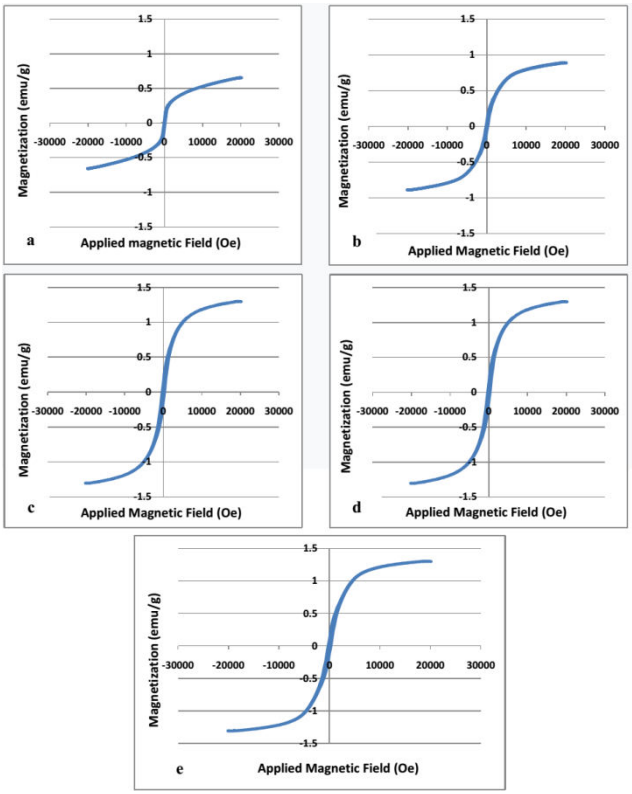

Figure-3. Hysteresis loop of iron oxide nanoparticles (a) undoped and cobalt doped (b) 5 wt.%, (c) 10 wt.%, (d) 15.wt % and (e) 20 wt.%.

Table-2. Hysteresis loop parameters of undoped and cobalt doped hematite nanoparticles.

Cobalt content (wt.%)	Magneti zation (emu/g)	Remanence Magneti zation (emu/g)	Coercivity (Oe)
0	0.65	0.095	124
5	0.89	0.098	221
10	1.28	0.168	255
15	1.29	0.171	299
20	1.30	0.145	269

Figure-4 shows the Touc graph for the indirect band gap energy transition for undoped and cobalt doped hematite nanoparticles. The band gap energy of undoped and cobalt doped hematite nanoparticles was determined using the following equation [24]:

$$(\alpha hv)^n = A(hv - Eg) \quad \ldots\ldots\ldots\ldots\ldots\ldots (2)$$

where α is the absorption coefficient, A is a constant, hv is the light energy and n is a constant that depends on the transition properties of the electron [25]. Hematite has n = 1/2 for the indirect band gap [26]. The band gap energy of both undoped and cobalt doped hematite nanoparticles can be determined from the graph of the relationship between $(\alpha hv)^2$ versus hv. The linear part of the graph with a certain slope where extrapolation when crossing the x-axis will produce the band gap energy. The band gap energy for undoped and cobalt doped 5, 10, 15 and 20 wt.% hematite nanoparticles as shown in Figure-4 are presented in Table-3. The value of this band gap energy decreases with the addition of the cobalt content. This band gap energy value remains in the range of 1.54 - 2.3 eV as shown in

reference [27]. These results indicate that the cobalt doped hematite nanoparticles exhibit photocatalytic properties under visible light irradiation.

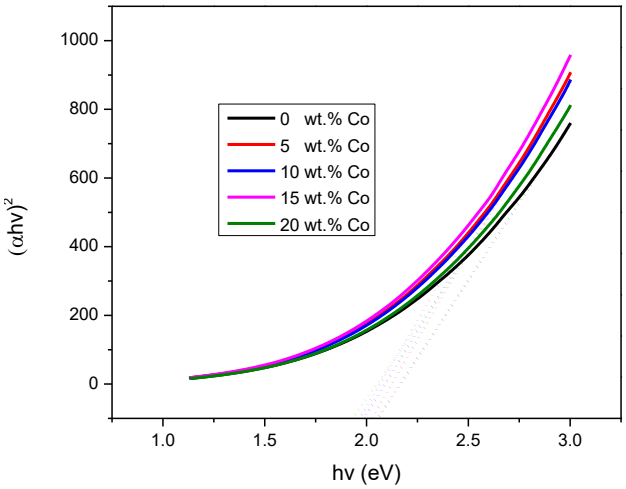

Figure-4. Tauc plot of undoped and cobalt doped hematite nanoparticles.

Table-3. Band gap energy (eV) for undoped and cobalt doped hematite nanoparticles.

Cobalt content (wt. %)	0	5	10	15	20
Band gap energy (eV)	2.07	2.03	1.98	1.96	1.93

CONCLUSIONS

In this study, cobalt doped hematite nanoparticles with different cobalt content (0, 5, 10, 15 and 20 wt.%) were prepared by ball milling method. The results of XRD measurement show that increasing amount of cobalt content results smaller crystallite size of hematite nanoparticles. High cobalt content (about 20 wt.%) shows an effective method to decrease the crystallite size of cobalt doped hematite nanoparticles. The crystal structure of hematite nanoparticles was unchanged after the introduction of cobalt. However, the magnetic properties of cobalt doped hematite nanoparticles were significantly affected. Magnetization (Ms) and remanance magnetization (Mr) increase with increasing amount of cobalt while, the coercivity of the samples increases with increasing cobalt content. Fe and Ti elements cannot be separated until 100 hours milling process suggesting that Fe and Ti exist in the form of compound. The band gap energy of hematite nanoparticles reduces by introducing cobalt as a doping element. The ability to modify hematite nanoparticles in controllable size and band gap energy may enable them to be used for environmental application.

ACKNOWLEDGMENTS

This work was financially supported by the Directorate General of Higher Education, Indonesian Ministry of Education, Culture, Research and Technology (Agreement no. 2596/UN.19.5.1.3/PT.01.03/2022. The authors are grateful to Indonesian Sciences Institute (LIPI), for conducting the VSM measurement and Department of Physics UNP for conducting the XRD and XRF measurements.

REFERENCES

[1] Erwin Amiruddin, Heri Hadianto, Martha Riana, Salomo Sinuraya, Mohammad Deri Noverdi and Ainun Syarifatul Fitri. 2021. Undoped and manganese doped iron oxide nanoparticles for environmental applications. ARPN Journal of Engineering and Applied Sciences. 16, 18, 1872-1876.

[2] Teja A. S. and Koh P. Y. 2009. Synthesis, properties, and applications of magnetic iron oxide nanoparticles Progress in Crystal Growth and Characterization of Materials. 5525-45.

[3] Xu P., Zeng G. M., Huang D. L., Feng C. L. Hu, S. Zhao M.H., Lai C., Wei Z., Huang C., Xie G.X., Liu Z.F. 2012. Use of iron oxide nanomaterials in wastewater treatment: A review. Sci. Total Environ. 424: 1-10.

[4] Liu J., Yang H., Xue X. 2019. Preparation of different shaped α−Fe2O3 nanoparticles with large particle of iron oxide red. Cryst. Eng. Comm. 21: 1097-1101.

[5] Akbarzadeh A., Samiei M., Davaran S. 2012. Magnetic nanoparticles: preparation, physical properties, and applications in biomedicine. Nanoscale Res. Lett. 7: 144.

[6] Wu W., Wu Z., Yu T., Jiang C., Kim W. S. 2015. Recent progress on magnetic iron oxide nanoparticles: synthesis, surface functional strategies and biomedical applications. Sci. Technol. Adv. Mater. 16: 023501.

[7] R. Araujo, A. Fiuza. 2015. The Use of nanoparticles in Soil and Water Remediation processes, Materials Today: proceedings. 2-1, 315-320.

[8] Tadica M., Panjan M., Damnjanovicc V., Milosevic I. 2014. Magnetic properties of hematite (α-Fe_2O_3) nanoparticles prepared by hydrothermal synthesis method. Appl Surf Sci. 320, 183-7.

[9] Quintin M., Devos O., Delville MH. 2006. Campet G Study of the lithium insertion-deinsertion mechanism in nanocrystalline γ-Fe2O3 electrodes by means of electrochemical impedance spectroscopy. Electrochim Acta. 51, 6426-6434.

[10] L. Hu, A. Percheron, D. Chaumont. 2011. Microwave-assisted one-step hydrothermal synthesis of pure iron oxide nanoparticles: magnetite, maghemite and hematite. 198-205.

[11] Amiruddin E. and Prayitno A. 2019. The synthesis of magnetic nanoparticles from natural iron sand of Kata beach Pariaman West Sumatera using ball milling method as environmental material MATEC Web of Conferences. 276: 06014.

[12] A. Erwin, S. Salomo, P. Adhy, N. Utari, W. Ayu, Y. Wita and S. Nani. 2020. Magnetic iron oxide particles (Fe_3O_4) fabricated by ball milling for improving the environmental quality. IOP Conf. Series: Materials Science and Engineering. 845: 012051.

[13] S. Razavi-Tousi and J. Szpunar. 2015. Effect of ball size on steady state of aluminium powder and efficiency of impacts during milling. Powder Technology. 284: 149-158.

[14] Erwin Amiruddin, Amir Awaluddin, Innike Hariani, Ribka Sihombing and Riska Angraini. 2020. The Influence of Milling Ball Size on the Structural, Morphological and Catalytic Properties of Magnetite (Fe3O4) Nanoparticles toward Methylene Blue Degradation. Journal of Physics: Conference Series 1655. 012006 doi:10.1088/1742-6596/1655/1/012006

[15] Heri Hadianto, Erwin Amiruddin, Rebi Septiawan, Putri Venera and Vivi Aprilia. 2020. Structural and Morphological Properties of Undoped and Manganese Doped Hematite Nanoparticles Prepared by Ball Milling Method. Journal of Physics: Conference Series 1655: 012013 doi:10.1088/1742-6596/1655/1/012013

[16] Krishnan K M, Pakhomov A B, Bao Y, Blomqvist P, Chun Y and Griffin K. 2006. Nanomagnetism and spin electronics: materials, microstructure and novel properties Journal of Materials Science. 41: 793-815.

[17] K. Supattarasakda, K. Petcharoen, T. Permpool, A. Sirivat W. 2013. Lerdwijitjarud, Powder Technol. 249: 353-359.

[18] Kyoung-Won Park, Alexie M. Kolpak. 2018. Journal of Catalysis. 365: 115-124.

[19] Caixia Xu, Fenglei Sun, Hua Gaob, Jinping Wanga. 2013. Nanoporous platinum-cobalt alloy for electrochemical sensing for ethanol, hydrogen peroxide, and glucose. J. Analytica Chimica Acta. 780: 20-27.

[20] J. Lin, Y. Lin. 2002. Hot-fluid annealing for crystalline titanium dioxide nanoparticles in stable suspension, J. Am. Chem. Soc. 124: 11514-11518, doi:http://dx.doi.org/10.1021/ja0206341. 12236766

[21] Lassoued A., Dkhil B., Gadri A., Ammar S. 2017. Control of the shape and size of iron oxide (α−Fe_2O_3) nanoparticles synthesized through the chemical precipitation method. Results Phys. 7: 3007-3015.

[22] R. Satheesh, K. Vignesh, A. Suganthi, M. Rajarajan. 2014. Visible light responsive photocatalytic applications of transition metal (M = Cu, Ni and Co) doped a-Fe_2O_3 nanoparticles. Journal of Environmental Chemical Engineering. 2: 1956-1968. http://dx.doi.org/10.1016/j.jece.2014.08.016

[23] Erwin and Adhy Pryayitno. 2017. Magnetic exchage interaction in cobalt samarium thin films for high density magnetic recording media. ARPN Journal of Engineering and Applied Sciences. 12, 12, 3832-3835.

[24] J. Tauc, R. Grigorovici, A. Vancu. 1966. Phys. Stat. Solidi. 15, 627-637.

[25] A. Lassoued, B. Dkhil, A. Gadri, S. Ammar. 2017. J. Results Phys. 7, 3007-3015.

[26] S.K. Bhar, N. Mukherjee, S. K. Maji, Synthesis of nanocrystalline iron oxide ultrathin films by thermal decomposition of iron nitropruside: structural andoptical properties, Mater. Res. Bull. 2010: 45, 1948-1953.

[27] Gilbert B., Frandsen C., Maxey er, Sherman DM. Band-gap measurements of bulk and nanoscale hematite by soft X-ray spectroscopy. Phys rev B 2009: 79, 35108-135108-7.